Available online at www.sciencedirect.com
ScienceDirect
Phytochemistry 67 (2006) 1781–1788
PHYTOCHEMISTRY
www.elsevier.com/locate/phytochem

Computation of the redox and protonation properties of quinones: Towards the prediction of redox cycling natural products

Jonathan L. Cape [a], Michael K. Bowman [a,b], David M. Kramer [a,*]

[a] Institute of Biological Chemistry, Washington State University, 289 Clark Hall, Pullman, WA 99164-6314, United States
[b] Structural Biology and Microimaging, Battelle Northwest Laboratories, Richland, WA 99354-0999, United States

Received 6 March 2006; received in revised form 9 June 2006
Available online 26 July 2006

Dedicated to Prof. Rodney Croteau on the occasion of his 60th birthday.

Abstract

Quinone metabolites perform a variety of key functions in plants, including pathogen protection, oxidative phosphorylation, and redox signaling. Many of these structurally diverse compounds have been shown to exhibit potent antimicrobial, anticancer, and anti-inflammatory properties, although the exact mechanisms of action are far from understood. Redox cycling has been proposed as a possible mechanism of action for many quinone species. Experimental determination of the essential thermodynamic data (i.e. electrochemical and pK_a values) required to predict the propensity towards redox cycling is often difficult or impossible to obtain due to experimental limitations. We demonstrate a practical computational approach to obtain reasonable estimates of these parameters.

Keywords: Hartree–Fock; Density functional theory; Quinone; Semiquinone; Quinol; Redox cycling; Superoxide; Reactive oxygen; Ubiquinone; Semiquinone stability constant; Electrochemistry

1. Introduction

Quinone metabolites serve vital roles in electron transport, pathogen defense, and as protein cofactors in nearly all forms of life (Thomas, 1971). The primary metabolites ubiquinone and plastoquinone function in the Mitchellian redox loops of mitochondrial and chloroplast electron transport chains (Cramer and Knaff, 1991; Trumpower, 1990; Cramer et al., 2005), coupling the chemical energy of reducing substrates (i.e. $NADH^+$ and succinate in mitochondria, or water oxidation in the case of photosynthesis) to the establishment of a proton motive force across the membrane to drive ATP synthesis. Some of these metabolites, e.g. ubiquinone, also act as potent antioxidants (Nohl et al., 2001).

Secondary quinone metabolites are also widespread throughout the plant, fungi, bacteria and animal kingdoms, encompassing a dizzying array of structurally diverse compounds which play defensive roles (allelopathic, antimicrobial etc.) for many organisms (Thomas, 1971). Well-characterized examples of this class in plants include the 1,4-naphthoquinone derivates such as jugalone, lawsone, and plumbagin (Thomas, 1971; Inbaraj and Chignell, 2004). Although the biological activity of these compounds have yet to be fully understood, at least some of their effects can be attributed to redox cycling, which redirects reducing equivalents in the cell towards detrimental superoxide production (Inbaraj et al., 1999a,b; Gutierrez, 2000; Inbaraj and Chignell, 2004; Rodriguez et al., 2004; Ding et al., 2005). Redox cycling can directly combat infection through the known toxicity of reactive oxygen species (Kramer et al., 2004; Rodriguez et al., 2004), or can act in signaling cascades to elicit other protective cellular measures, such as apoptosis (Liu, 1999; Petrosillo et al., 2001).

* Corresponding author.
E-mail address: dkramer@wsu.edu (D.M. Kramer).

0031-9422/$ - see front matter © 2006 Published by Elsevier Ltd.
doi:10.1016/j.phytochem.2006.06.015

Evaluating the propensity of quinone natural products to redox cycle is a critical component in elucidating mechanisms of biological activity. To date, this task has proven difficult due to a lack of information on specific quinone equilibria. The potential of quinone compounds to participate in redox cycling is mainly dependent on the stability of the semiquinone radical (SQ) relative to the quinone (Q) and quinol (QH_2) forms (i.e. how easy it is to form SQ through either the one electron reduction of Q or the one electron oxidation of QH_2). In principle, SQ stability can be estimated using the standard electrode potentials for the Q/QH_2 and $Q/Q^{\cdot-}$ redox couples and the pK_a of the SQ species (p$K_{a\,SQ}$).

Few complete studies have been performed on the equilibria of quinone natural products, excluding the obvious extensive work on ubiquinone and plastoquinone (Prince et al., 1983; Gunner et al., 1986; Wraight, 2004; Cape et al., 2005). Several studies have defined the Q/QH_2 and $Q/Q^{-\cdot}$ couples for betanins from *Opuntia ficus indica* in aqueous solution (Butera et al., 2002) and various flavinol glycosides and arylalkonic acids in non-aqueous solution (Silva et al., 2001; Corsino et al., 2003). The relationship between structure and redox potential for organic compounds, however, is not straightforward; therefore these values can rarely be generalized to other redox active organic species. In certain cases irreversible electrode kinetics completely prevents a reliable determination of the standard reduction potential (Silva et al., 2001; Butera et al., 2002). Additionally, standard electrochemical techniques cannot probe the pK_a of SQ species, thus preventing a full description of SQ reactivity.

In this work we demonstrate the practical use of quantum chemical calculations to predict the equilibria of quinone natural products. We show that the direct correlation of reaction free energies derived from gas phase Hartree–Fock (HF) and density functional theory (DFT) calculations with the corresponding experimental solution equilibrium constants provides an adequate description of SQ equilibria, thus providing order of magnitude estimates of SQ stability. These methods are potentially applicable to a wide range of organic redox active molecules, and can serve as a practical and powerful tool to predict redox cycling mechanisms for natural products.

The overall kinetic consequences of the quinone thermodynamic parameters investigated in this work will be treated in detail in a future manuscript. Our interest here is in making relative comparisons of reactivity within a series of compounds under controlled conditions.

2. Theory

A general redox cycling scheme is depicted in Scheme 1, which shows the formation of SQ from Q or QH_2 species, followed by the reduction of O_2 by both protonated and anionic states of SQ to form $O_2^{\cdot-}$ (Gutierrez, 2000; Roginsky and Barsukova, 2000; Rodriguez et al., 2004). In the following, we will sometimes purposely use the ambiguous term SQ to describe both protonation states, $QH^{\cdot}$ and $Q^{\cdot-}$, of SQ species. Both these species are highly reactive, although the anion is the most likely species to be observed at physiological pH. All these species can reach equilibrium with one another spontaneously, as shown by the double arrows connecting Q, SQ, and QH_2. In addition, certain enzyme systems can couple these redox transitions to other cellular processes, pulling the [SQ] out of equilibrium with Q and QH_2. These cases are more complex, but can be treated through an extension of the model discussed below.

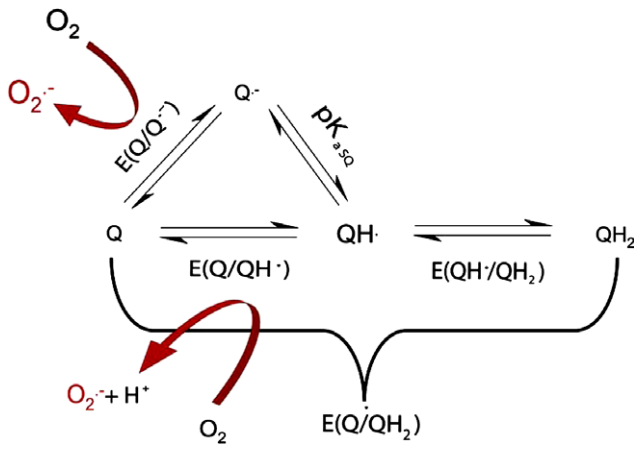

Scheme 1. Illustration of superoxide production from $Q^{\cdot-}$ and $QH^{\cdot}$, and thermodynamic cycles for the relevant equilibria involved in calculating K_S.

Here we consider the two essential equilibrium parameters that determine the rate of superoxide production by a quinone species (Afanas'ev, 1989): (1) the redox potential of the Q/SQ couple, which dictates the second order rate constant for superoxide production, and (2) the equilibrium constant for formation of SQ from Q and QH_2, also known as the SQ stability constant, K_S, which will dictate the total concentration of SQ at equilibrium. Typically, K_S is used to describe the propensity for formation of total SQ (i.e. both protonation states) by comproportionation of Q and QH_2 (Eq. 1).

$$K_S = \frac{[SQ]^2}{[QH_2][Q]} \tag{1}$$

Since the overall comproportionation reaction of Q and QH_2 involves the sum of two separate redox processes (i.e. the reduction of Q to $Q^{\cdot-}$ or $QH^{\cdot}$, and the oxidation of QH_2 to $Q^{\cdot-}$ or $QH^{\cdot}$), a simple expression for K_S can be derived by solving the relevant thermodynamic cycles. Eq. (2) and Scheme 1 show K_S for formation of the $QH^{\cdot}$ species, termed $K_S(QH^{\cdot})$, given in terms of the potentials for the $Q/Q^{\cdot-}$, Q/QH_2 couples, and p$K_{a\,SQ}$.

$$K_S(QH^{\cdot}) = \exp\frac{-2F[E(Q/QH_2) - E(Q/Q^{\cdot-}) - 0.059(pH - pK_{aSQ})]}{RT} \tag{2}$$

It is critical, however, to consider the effective stability constants for both protonation forms of SQ. Deprotonation of the neutral semiquinone (Eq. (3)) occurs at physiological pH, which generally has the effect of increasing the apparent stability constant due to the relatively low aqueous pK_a values (<6) of most known SQ species, thus resulting in Eq. (4) for $K_S(Q^{\cdot -})$

$$QH_2 + Q \overset{K_S(QH^{\cdot})}{\rightleftharpoons} 2QH^{\cdot} \overset{K_{aSQ}}{\rightleftharpoons} 2Q^{\cdot -} + 2H^+ \quad (3)$$

$$K_S(Q^{\cdot -}) = K_S(QH^{\cdot})(K_{aSQ})^2 = K_S(QH^{\cdot})10^{2(pH - pK_{aSQ})} \quad (4)$$

In general, superoxide production can occur through either the $QH^{\cdot}$ or the $Q^{\cdot -}$ species. Thus, the total SQ concentration ($[QH^{\cdot}] + [Q^{\cdot -}]$) needs to be taken into account, as shown in Eq. (5) (for simplicity in the final result we neglect the middle cross term $2[Q^{\cdot -}][H^+][QH^{\cdot}]/[Q][QH_2]$ in the expansion of $[SQ]^2$)

$$\begin{aligned} K_S(Q^{\cdot -} + QH^{\cdot}) &= \frac{[SQ]^2}{[QH_2][Q]} \\ &= \frac{[Q^{\cdot -}]^2[H^+]^2}{[Q][QH_2]} + 2\frac{[Q^{\cdot -}][H^+][QH^{\cdot}]}{[Q][QH_2]} \\ &\quad + \frac{[QH^{\cdot}]^2}{[Q][QH_2]} \\ &\approx K_S(QH^{\cdot})(10^{2(pH - pK_{aSQ})} + 1) \end{aligned} \quad (5)$$

A major experimental difficulty in evaluating this expression is in estimating the very low concentrations of reactive SQ species (Roginsky et al., 1999). An alternative approach would be to determine K_S from the redox potentials and pK_a values of the individual electron and protonation steps (Hong et al., 1999; Wraight, 2004; Cape et al., 2005). Unfortunately, this approach is also difficult since the $QH^{\cdot}$ species rapidly disproportionates in aqueous solution at physiological pH.

Quantum chemical calculations (Wheeler, 1994; Namazian, 2003; Namazian et al., 2003; Namazian and Almodarresieh, 2004; Namazian and Norouzi, 2004; Fu et al., 2005), in principle, can provide these values by calculating the total free energy of the relevant redox and acid/base half-cell reactions in the gas phase

$$Q\ (g) + H_2\ (g) \rightleftharpoons QH_2\ (g) \quad (6)$$

$$Q\ (g) \rightleftharpoons Q^{\cdot -}\ (g) \quad (7)$$

$$Q^{\cdot -}\ (g) + H^+\ (g) \rightleftharpoons QH^{\cdot}\ (g) \quad (8)$$

where Eq. (6), $E(Q/QH_2)_g$, is the two-electron hydrogenation of Q, Eq. (7), $E(Q/Q^{\cdot -})_g$, is the electron affinity of Q, and Eq. (8), $E(Q^{\cdot -}/QH^{\cdot})_g$ is the proton affinity of $Q^{\cdot -}$. Additional details of these calculations, including tables of the total free energy for all species, are provided in Supporting Information.

Ab initio estimates of reaction free energies such as these neglect solvation energy and other intermolecular interactions. These secondary interactions can be accounted for through continuum electrostatic treatments, yielding a completely ab initio potential (Namazian, 2003; Namazian et al., 2003; Namazian and Almodarresieh, 2004; Namazian and Norouzi, 2004; Fu et al., 2005). For practical applications, we suggest the simpler approach of directly correlating gas phase reaction free energies with experimental redox potentials at pH 7.0 to generate a calibration curve. Referencing the data with such a calibration curve is equivalent to comparing a half-cell reaction with a full electrochemical cell (in our case to the standard hydrogen electrode). While this approach is simplistic in nature compared to completely ab initio approaches, we show here that such approximations can yield remarkably accurate predictions for unknown compounds.

3. Results and discussion

3.1. Calculation of thermodynamic parameters

We have compiled the available aqueous electrochemical data on the one- and two-electron $Q/Q^{\cdot -}$ and Q/QH_2 couples (pH 7.0) and $pK_{a\ SQ}$ values for 18 selected quinone species (Fig. 1 and Supporting Information Table S2), including several well known natural products (2,6-dimethoxy-1,4-benzoquinone (**6**), 2-methyl-1,4-benzoquinone (**2**), ubiquinone-0 (**7**), plastoquinone-0 (**4**), and rhodoquinone (**8**)). This series encompasses mostly substituted 1,4-benzoquinones (**1**–**11**), but also includes some 1,4-naphthoquinone (1,4-naphthoquinone (**12**), 2-hydroxy-1,4-naphthoquinone (**13**), naphthazarin (**16**)), and anthraquinone (9,10-anthraquinone (**14**), 9,10-anthraquinone-2-sulfonate (**15**), and 1,4-dihydroxy-9,10-anthraquinone (**17**)) species as well. The range of experimental reduction potentials covered by this series is ~0.5 V for both the $Q/Q^{\cdot -}$ and Q/QH_2 couples, thus providing a reasonable range for testing our ability to predict experimental redox potentials.

Fig. 2 shows that DFT calculations using the popular B3LYP hybrid functional, in comparison with HF calculations, provides the best linear correlation between $E(Q/QH_2)_g$ (Eq. (6)) with the experimental potentials for the aqueous Q/QH_2 couple at pH 7.0. A linear correlation was obtained using B3LYP, with a slope of 0.875 (±0.097) and an offset of 0.221 (±0.017) eV ($R^2 = 0.890$) (Fig. 2, closed squares), compared with a slope of 1.904 (±0.395) and offset of −0.660 (±0.071) eV ($R^2 = 0.698$) (Fig 2, open circles), respectively, obtained using HF calculations. Interestingly, the inclusion of solvation effects tends to drastically improve agreement between theory and experiment for HF calculations, while having the opposite effect for B3LYP calculations (Namazian and Almodarresieh, 2004). In this work we find it unnecessary to include such solvent effects due to the good predictive power of the gas phase B3LYP calculations. Comparison between experimental and calculated Q/QH_2 potentials from the linear fit described above yields r.m.s. errors of 0.034 and 0.065 V for B3LYP/6-31G(d,p) and HF/6-31G(d,p) calculations, respectively. The quality of these predictions are

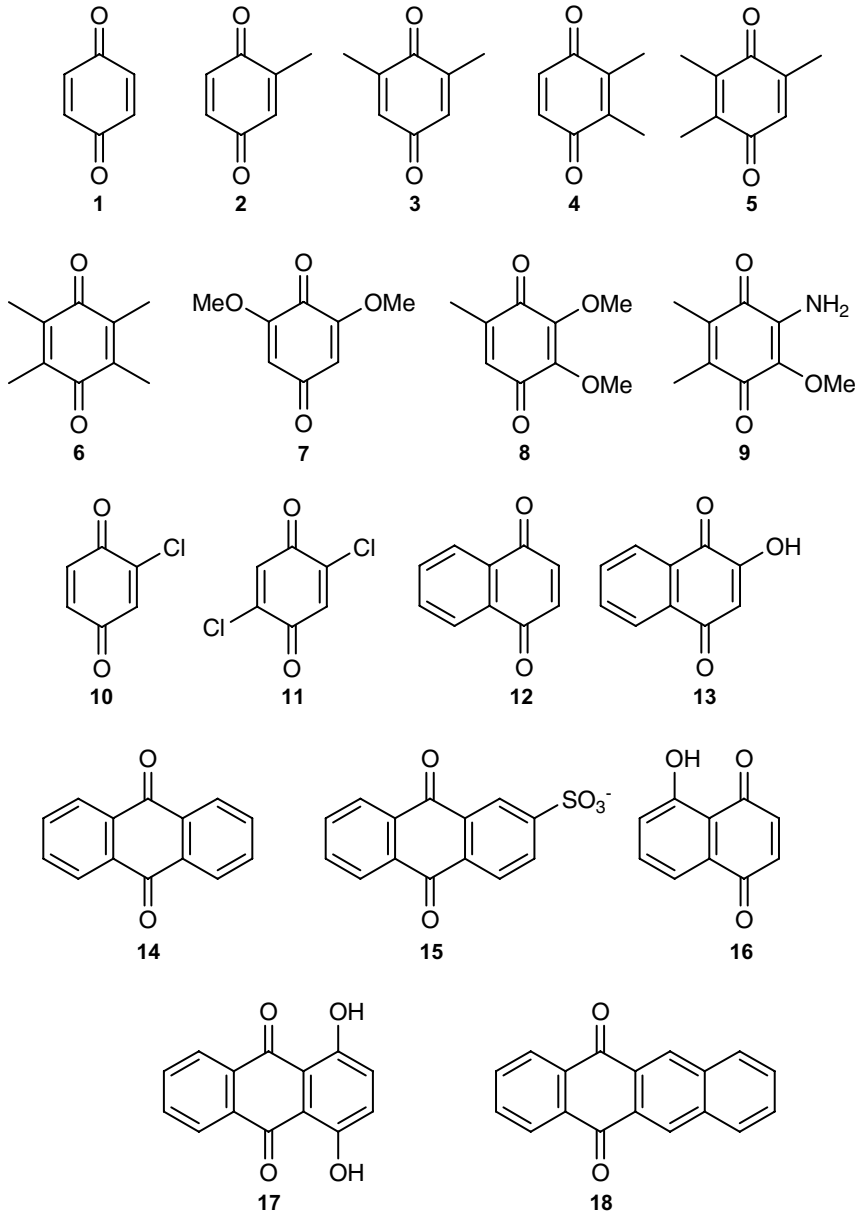

Fig. 1. Structures of the quinones studied in this work: 1,4-benzoquinone (**1**); 2-methyl-1,4-benzoquinone (**2**); 2,6-dimethyl-1,4-benzoquinone (**3**); 2,3-dimethyl-1,4-benzoquinone (**4**); 2,3,5-trimethyl-1,4-benzoquinone (*plastoquinone-0*) (**5**); 2,3,5,6-tetramethyl-1,4-benzoquinone (*duroquinone*) (**6**); 2,3-dimethoxy-5,6-dimethyl-1,4-benzoquinone (*ubiquinone-0*) (**7**); 2,6-dimethoxy-1,4-benzoquinone (**8**); rhodoquinone (**9**); 2-chloro-1,4-benzoquinone (**10**); 2,5-dichloro-1,4-benzoquinone (**11**); 1,4-naphthoquinone (**12**); 2-hydroxy-1,4-naphthoquinone (**13**); 9,10-anthraquinone (**14**); 9,10-anthraquinone-2-sulfonate (**15**); naphthazarin (**16**); 1,4-dihydroxy-9,10-anthraquinone (**17**); 5,12-naphthacenedione (**18**).

comparable with more computationally expensive methods, with Namazian and coworkers reporting 0.026 V for a set of eight Q/QH_2 (benzoquinone) species (Namazian and Almodarresieh, 2004), while Wass and coworkers report 0.006 V r.m.s. error for their limited set of three (benzoquinone) Q/QH_2 species (Wass et al., 2005).

In contrast to the available experimental data on the Q/QH_2 couple, few determinations of the $Q/Q^{\cdot-}$ couple in aqueous solution have been reported, mainly due to the uncertainties about whether one is observing the $Q/Q^{\cdot-}$ or Q/QH_2 couple. This couple, however, can be obtained by performing electrochemical experiments in unbuffered aqueous solution, where at high pH the kinetics of the $Q/Q^{\cdot-}$ electron transfer out-compete protonation of $Q^{\cdot-}$ at the electrode surface (Shim and Park, 1997; Cape et al., 2005). We used cyclic voltammetry under these conditions to compile an experimental data set for a series of readily available quinones (see Supporting Information Table S2) and compared these values to similar calculations as described above for the $Q/Q^{\cdot-}$ couple in the gas phase.

Fig. 3 shows linear relationships between $E(Q/Q^{\cdot-})_g$ (Eq. (7)) and the experimental aqueous $Q/Q^{\cdot-}$ potentials for both B3LYP and HF calculations. The B3LYP results yield a slope of 0.93 and an offset of 1.54 eV ($R^2 = 0.61$)

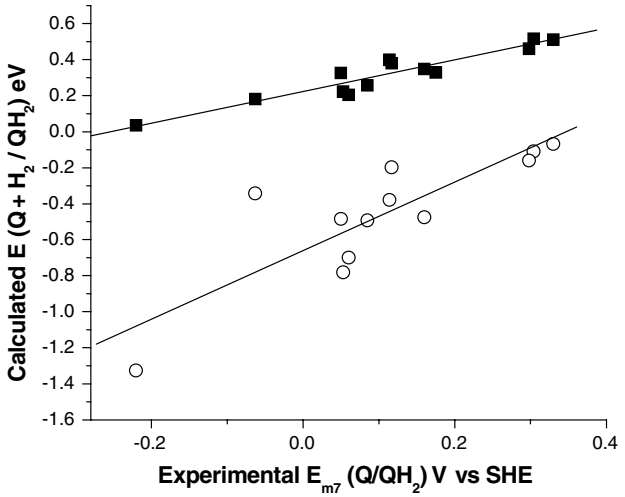

Fig. 2. Correlation of the gas phase hydrogenation free energy of Q to QH_2 (Eq. (6)) (eV) to aqueous two-electron reduction potentials (V vs. SHE) at pH 7.0. Calculations were performed at the B3LYP/6-31G(d,p) (black squares) and HF/6-31G(d,p) (open circles) levels of theory. Linear fits are shown as solid lines; $E(Q/QH_2)_g = 0.875[E_{m7}(Q/QH_2)] + 0.221$ eV for calculations performed using B3LYP/6-31G(d,p), and $E(Q/QH_2)_g = 1.904[E_{m7}(Q/QH_2)] - 0.660$ eV for calculations performed using HF/6-31G(d,p). Quinones used in this correlation are (from highest to lowest potential): **11**, **10**, **1**, **2**, **4**, **3**, **8**, **5**, **12**, **6**, **7**, **9**, and **13**. Details of the calculations and quinone potentials can be found in the Theory and Supporting Information sections.

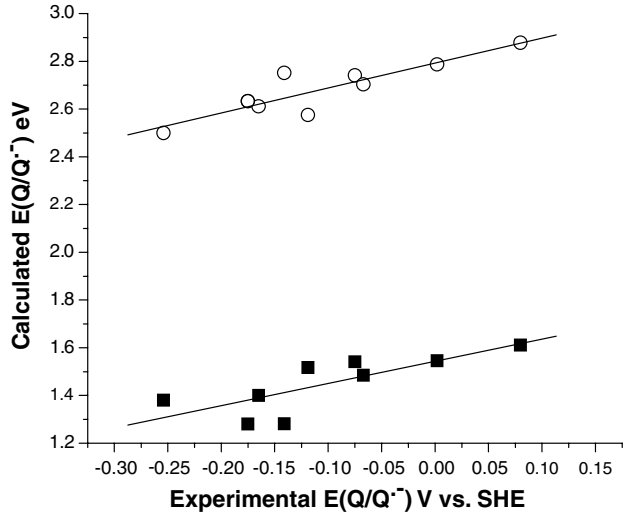

Fig. 3. Correlation of gas phase electron affinities (Eq. (7)) (eV) to aqueous one-electron reduction potentials of Q–$Q^{\cdot-}$ (V vs. SHE). Calculations were performed at the B3LYP/6-31G(d,p) (black squares) and HF/6-31G(d,p) (open circles) levels of theory. Linear fits are shown as solid lines; $E(Q/Q^{\cdot-})_g = 0.93[E_m(Q/Q^{\cdot-})] + 1.54$ eV for calculations performed using B3LYP/6-31G(d,p), and $E(Q/Q^{\cdot-})_g = 1.04[E_m(Q/Q^{\cdot-})] + 2.79$ eV for calculations performed using HF/6-31G(d,p). Quinones used in this correlation are (from highest to lowest potential): **1**, **2**, **3**, **8**, **12**, **7**, **5**, **9**, and **6**. Details of the calculations and quinone potentials can be found in the Theory and Supporting Information sections.

(Fig. 3, closed squares). HF calculations yield comparable results, with a slope of 1.04 and an offset of 2.79 eV ($R^2 = 0.79$) (Fig. 3, open circles). Two notable deviations from this relationship were observed for halogenated benzoquinones (2-chloro-1,4-benzoquinone (**9**) and 2,5-dichloro-1,4-benzoquinone (**10**)), whose $Q/Q^{\cdot-}$ potentials were greatly overestimated (data not shown). Although the origin of this deviation is presently unknown, we suggest it might be rectified through the use of larger basis sets or the inclusion of solvation effects. These values were therefore not included in the present fitting analysis, although can be reasonably fit using the same method if treated separately from non-halogenated benzoquinones (see Information Table S2). The $E(Q/Q^{\cdot-})$ values calculated here also exhibit excellent agreement with determinations of $E(Q/Q^{\cdot-})$ performed in acetonitrile (data not shown). Comparison between calculated and experimental $E(Q/Q^{\cdot-})$ values yields r.m.s. errors comparable to more expensive techniques; 0.059 and 0.016 V for B3LYP/6-31G(d,p) and HF/6-31G(d,p), respectively. Namzian and coworkers report r.m.s. values averaging 0.053 V in three different calculations of the $Q/Q^{\cdot-}$ couple using B3LYP in different solvents (DMSO, acetonitrile) (Namazian, 2003; Namazian et al., 2003; Namazian and Norouzi, 2004).

Fig. 4 shows a linear correlation between the calculated $\log K_{eq}$ for the gas phase proton affinity, $\log K_{eq}(Q^{\cdot-}/QH^{\cdot})$, and experimental $pK_{a\ SQ}$ values. Here $E(Q^{\cdot-}/QH^{\cdot})$ from Eq. (8) is converted into the logarithm of the equilibrium constant for comparison with pK_a values. Literature reports of experimental $pK_{a\ SQ}$ values for semiquinone species are scant due to the extreme instability of the protonated SQ species, which undergoes disproportionation to Q and QH_2 at near diffusion-limited rates. For the quinone species examined here, regardless of extended ring structures, experimental $pK_{a\ SQ}$ values lie within a small range, from approximately 2–6, with most benzosemiquinone $pK_{a\ SQ}$ values falling in the narrow range of 4–5.

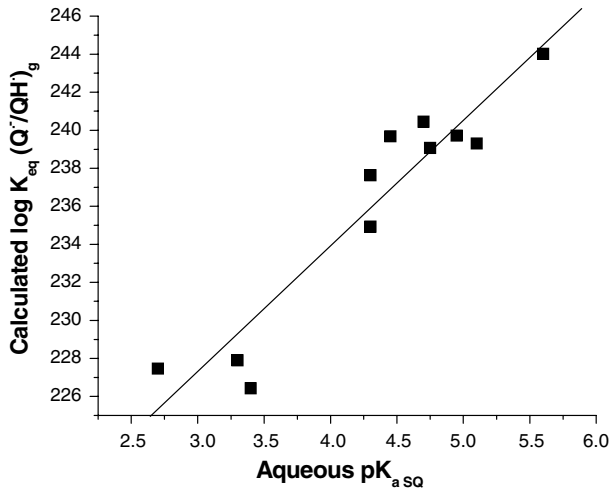

Fig. 4. Correlation of the $\log K_{eq}$ proton affinities of $Q^{\cdot-}$ (Eq. (8)) to aqueous $pK_{a\ SQ}$ values. Calculations were performed at the B3LYP/6-31G(d,p) level of theory. A linear fit is shown by the solid line; $\log K_{eq}(Q^{\cdot-}/QH^{\cdot})_g = 6.6[pK_{a\ SQ}] + 207.4$. Quinones used in this correlation are (from highest to lowest pK_a): **7**, **5**, **4**, **1**, **2**, **12**, **18**, **15**, **17**, and **16**. Details of the calculations and semiquinone pK_a values can be found in the Theory and Supporting Information sections.

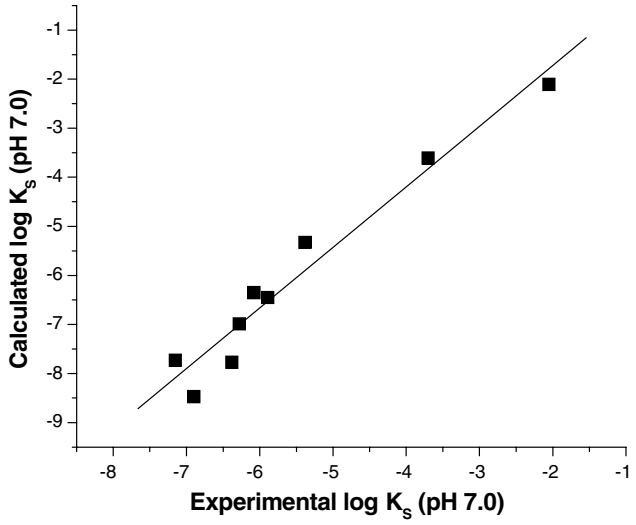

Fig. 5. Comparison of calculated and experimentally determined $\log K_S(Q^{\cdot-} + QH^{\cdot})$ values. A linear fit to the data yields $\log K_S(Q^{\cdot-} + QH^{\cdot}) = 1.23[\log K_{S\ exp}] + 0.74$. Experimentally determined values were taken from (Roginsky et al., 1999) (corrected to pH 7.0 and 23 °C) and (Cape et al., 2005).

Correlation of $\log K_{eq}(Q^{\cdot-}/QH^{\cdot})_g$ and $pK_{a\ SQ}$ for benzoquinones, naphthoquinone and anthraquinone species using B3LYP yields a slope of 6.6 and a vertical offset of 207.4 ($R^2 = 0.89$) (Fig. 4, closed squares). The use of HF yields a less robust correlation of $K_{eq}(Q^{\cdot-}/QH^{\cdot})_g$ and $pK_{a\ SQ}$ (data not shown) with poor agreement between calculated and experimental values and an apparent ring-structure dependence on calculated values; no fitting was attempted for this series due to the overall poor quality of the correlation. The r.m.s. error between experimental and calculated pK_a values was 0.36.

3.2. Prediction of K_S values

Fig. 5 compares $\log K_S(Q^{\cdot-} + QH^{\cdot})$ values calculated in this work to the experimentally determined values using electron paramagnetic resonance reported by Roginsky and coworkers (Roginsky et al., 1999). Redox potentials and $pK_{a\ SQ}$ values provided by the computational approach applied to Eqs. (2)–(5) provided excellent agreement with the absolute value of experimental $\log K_S(Q^{\cdot-} + QH^{\cdot})$ values ($R^2 = 0.95$, and an r.m.s. error between experimental and calculated values of 0.89) over a range of approximately seven orders of magnitude. The small error reported here is remarkable considering that the error in each individual redox potential or pK_a value propagates in a multiplicative manner when estimating $K_S(Q^{\cdot-} + QH^{\cdot})$.

4. Conclusions

We describe a simple and practical method for calculating thermodynamic parameters necessary to estimate semiquinone stability constants and redox potentials for quinone natural products. Our results indicate that a combination of different computationally inexpensive quantum chemical methods provide reasonable agreement with experiment. We recommend using HF/6-31G(d,p) for the calculation of $E(Q/Q^{\cdot-})$, and using B3LYP/6-31G(d,p) for calculation of $E(Q/QH_2)$ and $pK_{a\ SQ}$. The accuracy of these methods are comparable to approaches employing continuum solvation models and large basis sets, yet can be applied to a model system at modest computational expense. Improvements in the level of theory and in availability of experimental data should allow for improvements in such predictions. We do suggest, however, that care be taken in applying this type of empirical approach to a structurally disparate series due to the potential for large errors as the result of solvation energy neglect or basis set effects. Overall, the main advantage of the present approach, though, is that is can be readily applied to high throughput in silico screening of potential redox cycling agents.

5. Experimental and computational details

5.1. Cyclic voltammetry and determination of redox potentials

Voltammetric measurements of the $Q/Q^{\cdot-}$ couples for the series of quinones calculated were performed in aqueous solution under an Ar atmosphere at 23 °C using a BAS C50-W potentiostat (Bioanalytical Systems, West Lafayette, IN) with an Ag/AgCl reference electrode, glassy carbon working electrode, and Pt wire auxiliary electrode. The working electrode was washed with dilute H_2SO_4, repeatedly rinsed with distilled water, and then polished with alumina prior to all measurements. Determination of $E(Q/Q^{\cdot-})$ was performed in unbuffered solution (100 mM KCl) as described in Shim and Park (Shim and Park, 1997) at pH > 5.0. Aqueous $E(Q/Q^{\cdot-})$ values were determined at several pH values above pH 5.0 to insure that the $E_{1/2}$ and ΔE values were independent of pH, and thus reflect a pure electron transfer process. All experimental potentials given in the text are referenced to the standard hydrogen electrode. The quinones investigated by cyclic voltammetry (2,5-dichloro-1,4-benzoquinone (**10**); 2-chloro-1,4-benzoquinone (**9**); 1,4-benzoquinone; 2-methyl-1,4-benzoquinone (**2**); 2,6-dimethyl-1,4-benzoquinone (**3**); 2,3,5-trimethyl-1,4-benzoquinone (plastoquinone-0) (**4**), duroquinone (**5**), 2,3-dimethoxy-5-methyl-1,4-benzoquinone (ubiquinone-0) (**7**), 2,6-dimethoxy-1,4-benzoquinone (**6**); 1,4-naphthoquinone (**12**)) were obtained from Aldrich and used without further purification. All other relevant redox potentials and pK_a values were taken from the literature sources (see Table S2 of Supporting Information).

5.2. Computational details

Free energy values (i.e. the sum of the total electronic energy and Gibbs free energy correction) for each species

used in the calculation of redox potentials and proton affinity were taken from the output of combined optimization/frequency calculations in the Gaussian '03 suite of programs (see Supporting Information section S1 and Tables S4–S7). All calculations were performed at either the HF/6-31G(d,p) and B3LYP/6-31G(d,p) levels of theory.

Acknowledgements

We thank Drs. James Hurst, Marilyn Gunner, Wolfgang Nitschke, Aurora Clark, and Isaac Forquer for stimulating discussions regarding this manuscript. This work was supported by the National Institutes of Health, GM61904 (M.K.B.) and US Department of Energy DE-FG03-98ER20299 (D.M.K.). Part of this work was performed at the W.R. Wiley Environmental Molecular Sciences Laboratory, a national scientific user facility sponsored by the US Department of Energy's Office of Biological and Environmental Research and located at Pacific Northwest National Laboratory, operated by Battelle for DOE.

Appendix A. Supplementary data

Supplementary data associated with this article can be found, in the online version, at doi:10.1016/j.phytochem.2006.06.015.

References

Afanas'ev, I.B., 1989. Superoxide Ion: Chemistry and Biological Implications. CRC Press, Boca Raton, FL.

Butera, D., Tesoriere, L., Di Gaudio, F., Bongiorno, A., Allegra, M., Pintaudi, A.M., Kohen, R., Livrea, M.A., 2002. Antioxidant activities of sicilian prickly pear (*Opuntia ficus indica*) fruit extracts and reducing properties of its betalains: betanin and indicaxanthin. J. Agric. Food Chem. 50, 6895–6901.

Cape, J.L., Strahan, J.R., Lenaeus, M.J., Yuknis, B.A., Le, T.T., Shepherd, J.N., Bowman, M.K., Kramer, D.M., 2005. The respiratory substrate rhodoquinol induces Q-cycle bypass reactions in the yeast cytochrome bc_1 complex: mechanistic and physiological implications. J. Biol. Chem. 280, 34654–34660.

Corsino, J., Silva, D.H., Zanoni, M.V., da Silva Bolzani, V., Franca, S.C., Pereira, A.M., Furlan, M., 2003. Antioxidant flavan-3-ols and flavonol glycosides from *Maytenus aquifolium*. Phytother. Res. 17, 913–916.

Cramer, W.A., Knaff, D.B., 1991. Energy transduction in biological membranes. Springer-Verlag, New York, pp. 78–238.

Cramer, W.A., Yan, J., Zhang, H., Kurisu, G., Smith, J.L., 2005. Structure of the cytochrome b6f complex: new prosthetic groups, Q-space, and the 'hors d'oeuvres hypothesis' for assembly of the complex. Photosynth. Res. 85, 133–143.

Ding, Y., Chen, Z.J., Liu, S., Che, D., Vetter, M., Chang, C.H., 2005. Inhibition of Nox-4 activity by plumbagin, a plant-derived bioactive naphthoquinone. J. Pharm. Pharmacol. 57, 111–116.

Fu, Y., Liu, L., Yu, H.Z., Wang, Y.M., Guo, Q.X., 2005. Quantum-chemical predictions of absolute standard redox potentials of diverse organic molecules and free radicals in acetonitrile. J. Am. Chem. Soc. 127, 7227–7234.

Gunner, M.R., Robertson, D.E., Dutton, P.L., 1986. Kinetic studies on the reaction center protein from *Rhodopseudomonas sphaeroides*: the temperature and free energy dependence of electron transfer between various quinones in the Q_A site and the oxidized bacteriochlorophyll dimer. J. Phys. Chem. 90, 3783–3795.

Gutierrez, P.L., 2000. The metabolism of quinone-containing alkylating agents: free radical production and measurement. Front. Biosci. 5, D629–D638.

Hong, S., Ugulava, N., Kuras-Guergova, M., Crofts, A.R., 1999. The energy landscape for ubihydroquinone oxidation at the Q_o site of the bc_1 complex in *Rhodobacter sphaeroides*. J. Biol. Chem. 274, 33931–33944.

Inbaraj, J.J., Chignell, C.F., 2004. Cytotoxic action of juglone and plumbagin: a mechanistic study using HaCaT keratinocytes. Chem. Res. Toxicol. 17, 55–62.

Inbaraj, J.J., Gandhidasan, R., Murugesan, R., 1999a. Cytotoxicity and superoxide anion generation by some naturally occurring quinones. Free Radical Biol. Med. 26, 1072–1078.

Inbaraj, J.J., Krishna, M.C., Gandhidasan, R., Murugesan, R., 1999b. Cytotoxicity, redox cycling and photodynamic action of two naturally occurring quinones. Biochim. Biophys. Acta 1472, 462–470.

Kramer, D.M., Roberts, A.G., Muller, F., Cape, J., Bowman, M.K., 2004. Q-cycle bypass reactions at the Qo site of the cytochrome bc_1 (and related) complexes. Methods Enzymol. 382, 21–45.

Liu, S.S., 1999. Cooperation of a "reactive oxygen cycle with the Q cycle and the proton cycle in the respiratory chain–superoxide generating and cycling mechanisms in mitochondria. J. Bioenerg. Biomembr. 31, 367–376.

Namazian, M., 2003. Density functional theory response to the calculation of electrode potentials of quinones in non-aqueous solution of acetonitrile. J. Mol. Struct. (Theochem) 664–665, 273–278.

Namazian, M., Almodarresieh, H.A., 2004. Computational electrochemsitry: aqueous two-electron reduction potentials for substituted quinones. J. Mol. Struc. (Theochem) 686, 97–102.

Namazian, M., Norouzi, P., 2004. Prediction of one-electron electrode potentials of some quinones in dimethylsulfoxide. J. Electroanal. Chem. 573, 49–53.

Namazian, M., Norouzi, P., Ranjbar, R., 2003. Prediction of electrode potentials of some quinone derivatives in acetonitrile. J. Mol. Struct. (Theochem) 625, 235–241.

Nohl, H., Kozlov, A.V., Staniek, K., Gille, L., 2001. The multiple functions of coenzyme Q. Bioorg. Chem. 29, 1–13.

Petrosillo, G., Ruggiero, F.M., Pistolese, M., Paradies, G., 2001. Reactive oxygen species generated from the mitochondrial electron transport chain induce cytochrome *c* dissociation from beef-heart submitochondrial particles via cardiolipin peroxidation. Possible role in apoptosis. FEBS Lett. 509, 435–438.

Prince, R.C., Dutton, L., Bruce, J.M., 1983. Electrochemistry of ubiquinones. FEBS Lett. 160, 273–276.

Rodriguez, C.E., Shinyashiki, M., Froines, J., Yu, R.C., Fukuto, J.M., Cho, A.K., 2004. An examination of quinone toxicity using the yeast *Saccharomyces cerevisiae* model system. Toxicology 201, 185–196.

Roginsky, V.A., Barsukova, T., 2000. Kinetics of oxidation of hydroquinones by molecular oxygen. Effect of superoxide dismutase. J. Chem. Soc., Perkin Trans., 21575–21582.

Roginsky, V.A., Pisarenko, L.M., Bors, W., Michel, C., 1999. The kinetics and thermodynamics of quinone–semiquinone–hydroquinone systems under physiological conditions. J. Chem. Soc., Perkin Trans. 2, 871–876.

Shim, Y.B., Park, S.M., 1997. Spectroelectrochemical studies of *p*-benzoquinone reduction in aqueous media. J. Electroanal. Chem. 425, 201–207.

Silva, D.H., Pereira, F.C., Zanoni, M.V., Yoshida, M., 2001. Lipophyllic antioxidants from *Iryanthera juruensis* fruits. Phytochemistry 57, 437–442.

Thomas, R.H., 1971. Naturally Occurring Quinones. Academic Press, New York, NY.

Trumpower, B.L., 1990. Cytochrome bc_1 complexes of microorganisms. Microbiol. Rev. 54, 101–129.

Wass, J.R., Ahlberg, E., Panas, I., Schiffrin, D.J., 2005. Quantum chemical modeling of reduction of quinones. J. Phys. Chem. A 110, 2005–2020.

Wheeler, R.A., 1994. A method for computing one-electron reduction potentials and its application to *p*-benzoquinone in water at 300 K. J. Am. Chem. Soc. 116, 11048–11051.

Wraight, C.A., 2004. Proton and electron transfer in the acceptor quinone complex of photosynthetic reaction centers from *Rhodobacter sphaeroides*. Front. Biosci. 9, 309–337.